Physica B 739 (2026) 418940

Contents lists available at ScienceDirect

Physica B: Condensed Matter

journal homepage: www.elsevier.com/locate/physb

Superconducting diode effect in a two-dimensional mesoscopic film with asymmetric edge defects

C.A. Aguirre [a,*], Julián Faúndez [b], S.A. Acosta-Díaz [c], C.E. Martínez-Torres [c], J. Barba-Ortega [c]

[a] Departamento de Física, Universidad Distrital Francisco José de Caldas, Bogotá, Colombia
[b] Departamento de Física y Astronomía, Universidad Andres Bello, Santiago, Chile
[c] Departamento de Física, Universidad Nacional de Colombia, Bogotá, Colombia

ARTICLE INFO

Keywords:
Superconductor film
Diode effect
Critical current
Efficiency factor
External current
External magnetic field

ABSTRACT

This work presents an analysis of a superconducting sample with rectangular geometry, containing a semicircular defect, in which, over the angular range of 0° to 90°, there is a sinusoidal-type radial contribution. The system was simulated by numerically solving the time-dependent Ginzburg–Landau nonlinear equations, and an initial exploration of the vortex dynamics was conducted by varying the external magnetic field and one geometric parameter of the sample (bridge width). Subsequently, by applying currents first in one direction of the sample and then in the opposite direction, voltage–current curves (V–I) were obtained for two scenarios: in the first, the external magnetic field was varied while the film geometry was kept constant; in the second, the field was fixed, and one of the representative lengths of the sample was varied. In both cases, a difference was observed in the behavior of the critical currents for each polarity, as well as a dependence on the difference with the different parameters, allowing the determination of the diode-efficiency factor ($\gamma(H), \gamma(\mathbf{J})$) as a function of the parameter relevant to each situation. The values obtained demonstrate the potential of this geometry as a two-dimensional superconducting diode, which can be realized by breaking symmetry, without the need for complex Josephson-type couplings or the high manufacturing costs proposed in current works.

1. Introduction

It is undeniable that the last few decades have witnessed an unprecedented technological leap. This leap has impacted all areas of modern society and allowed the discovery and development of new techniques, as well as the analysis of phenomena and data that were previously unimaginable [1–5]. However, it is also important to note that this technological model, which has enabled these advances, presents significant challenges. These are mainly related to energy consumption and the inherent limitations of the semiconductors on which current digital systems are based [6–12]. Therefore, it is undeniable that we are on the verge of a new technological leap. This change has been developing over the past few years, driven by the discovery and implementation of superconducting systems [13–16]. These systems appear poised to replace current digital circuits. This is mainly due to their unique properties, which enable more efficient data processing and reduced energy losses [1–3,6,8,12–15]. The properties of these superconducting systems depend strongly on the type of superconductor [16–18]. If it is a Type I superconductor, the system completely shields the external field (Meissner effect) and behaves as a perfect diamagnetic system [1,2,5,7]. In the case of the so-called Type II superconductors, they allow quantized influx of vortices (the mixed state) and coexistence of both states [16,17]. Now, with the ultimate goal of exploiting the unique properties of this exotic state of matter, circuit elements based on different coupling techniques between superconducting condensates have been developed in recent years [19–23]. Most are in multi-band extensions (interactions between condensates) via Josephson-type interactions [24–26], weak interactions, or strong coupling, which involve complex interactions between the order parameters and their phase.

Thus, in recent years, the idea has emerged that symmetry breaking in superconducting systems can give rise to asymmetric behavior in certain electronic variables. It is well known that superconducting samples with broken time-reversal and inversion symmetries can exhibit different critical currents (I_c) depending on the bias polarity; i.e., there are cases where the dissipation-less super-current can flow in one direction but is blocked in the other. This effect, analogously to the similar situation that occurs in p-n semiconductor junctions, is appropriately named

* Corresponding author.
E-mail address: cristian@fisica.ufmt.br (C.A. Aguirre).

https://doi.org/10.1016/j.physb.2026.418940
Received 17 April 2026; Received in revised form 8 June 2026; Accepted 9 June 2026
Available online 23 June 2026
0921-4526/© 2026 Elsevier B.V. All rights are reserved, including those for text and data mining, AI training, and similar technologies.

the superconducting diode effect (**SDE**) [27]. **SDE** is growing in experimental and theoretical interest thanks to its wide range of applications. It single-handedly opens the door to non-dissipative electronics, as evidenced by this recent investigation focused on building real, usable components such as full-wave rectifiers [28,29] and memories [30–32] for quantum circuitry and spintronics, including new manufacturing techniques for nanomaterials, based on electron-beam lithograph and directed sputtering that have allowed the manufacturing of highly complex systems, with minimal errors of around $\pm n$m [33–36]. One of the most interesting points is the diverse theories used to study this important phenomenon. Although mid-field extensions have yielded results, the theory most successfully applied in these extensions, which allows for a quantitative description of the vortex state and its effect on the so-called super-current, is that of Ginzburg–Landau, which has made it possible to understand how the vortex state has an impact on the **SDE**. quite successfully. Symmetry breaking can be achieved solely through geometric artifacts and an external magnetic field. In light of this mechanism, it becomes necessary to study, understand, and develop accurate methods to predict the consequences of boundary defects on critical currents, to avoid them when undesired, or to exploit them to achieve desired efficiencies. However, reliable simulation of surface irregularities helps advance **SDE** technological applications.

In the present work, the geometry selected for this task was a rectangular slab with semicircular and radial-sine-type irregularities. Similar work has been done on periodic defects [37,38]. This design reveals differences in vortex nucleation, entry, and motion as a function of bias polarity. Thus, it demonstrates its usefulness in manifesting the effect. The main innovation here is to locate the defect by introducing a semicircle that encloses the indentations, rather than allowing them to fill one side of the slab. This approach introduces a geometric parameter to adjust efficiency, called the "bridge width". The numerical results will show that the optimal values of this parameter can achieve SDE efficiencies exceeding 20%. This paper is organized as follows. Section 2 describes the theoretical framework, including the time-dependent Ginzburg–Landau equations used in our analysis (Dirty limit). Section 3.1 presents the main results of our numerical simulations on electronic and superconductor variables. The results of three variations are discussed in Section 3.2. Finally, we summarize our conclusions and outline future directions in Section 4.

2. Theory and model

The sample studied in this paper corresponds to a rectangular thin film of size $a \times b$, whose thickness, denoted by c, is much smaller than the coherence length ($c \ll \xi$). The model also has a semicircular defect of radius R on one side, with radial variation following a sine function over the range 0° to 90°. This sample is subjected to a constant applied magnetic field H perpendicular to the $a-b$ plane and an applied bias current density $\mathbf{J}$ (positive current parallel to the y-axis and negative current, anti-parallel to the same axis). These directions, the position of the electrodes, and the described geometrical parameters are depicted in Fig. 1, where there is also a description of the specific functional form of the radial defect and a parameter denoted by d, which will be called "bridge width".

To describe the non-equilibrium dynamics of the superconducting state, we employ the generalized time-dependent Ginzburg–Landau (**TDGL**) formalism in the dirty limit [24,26,39–44]. These expressions are obtained after functionally deriving the Gibbs free energy functionals with respect to ψ and $\mathbf{A}$. In dimensionless form, the evolution of the complex superconducting order parameter $\psi(\mathbf{r},t)$ is governed by [45–49]:

$$\frac{1}{\sqrt{1+\Gamma^2|\psi|^2}}\left(\frac{\partial\psi}{\partial t}+i\Phi\psi+\frac{\Gamma^2}{2}\frac{\partial|\psi|^2}{\partial t}\psi\right)= \left(-i\nabla-\mathbf{A}\right)^2\psi+\psi\left(1-|\psi|^2\right), \tag{1}$$

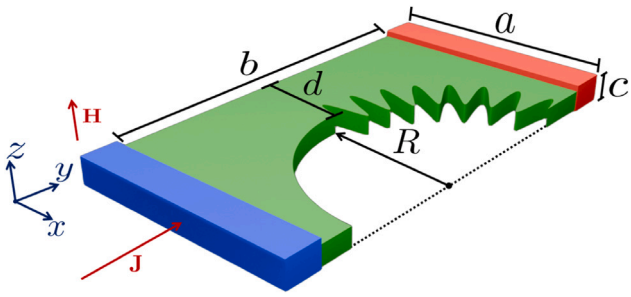


Fig. 1. A schematic representation of the sample: In green, the superconductor sample, in red and blue, the metallic electrodes. The dimensions of the sample are: $c \ll \xi(0)$, $b = 3.2\,\xi(0)$, $R = 0.6\,\xi(0)$, while the side length a is varied throughout this work. The radial defect can be expressed with the function $r(\theta) = R + r_0 \sin(\omega_0\theta)$, with parameters $r_0 = 0.1\,\xi(0)$ and $\omega_0 = 45/\xi(0)$, and θ is measured from the center of the semicircle. The bridge width d is defined as the difference between a and R ($d = a - R$). An external positive current $\mathbf{J}$ in the y-direction and a magnetic field H in the $\hat{z}$-direction.

Here, $\mathbf{A}(\mathbf{r},t)$ denotes the vector potential and $\Phi(\mathbf{r},t)$ is the scalar potential. The parameter $\Gamma = 10$ characterizes the relaxation dynamics of the superconducting condensate in our case [43,44]. The gauge-invariant kinetic operator, introduced via the covariant derivative $\mathbf{D} = -i\nabla - \mathbf{A}$, leads to the total current density: $\mathbf{J} = \mathrm{Re}\,[\psi^*(-i\nabla - \mathbf{A})\psi] - \nabla\Phi,$. This accounts for both the super-current due to Cooper-pair motion and the applied external current, which includes both superconducting and normal components. The vector potential evolves according to Maxwell's equation [45,46,48].

$$\frac{\partial\mathbf{A}}{\partial t} = \mathbf{J} - \kappa^2\nabla\times\nabla\times\mathbf{A}, \tag{2}$$

The Ginzburg–Landau parameter is given by $\kappa = \lambda/\xi$ [15,18,23]. This parameter determines the type of superconductor: $\kappa < 1/\sqrt{2}$ corresponds to type-I superconductors, while $\kappa > 1/\sqrt{2}$ corresponds to type-II superconductors. In our case, $\kappa = 2.0$. To proceed with our analysis, we adopt the Coulomb gauge, $\nabla\cdot\mathbf{A} = 0$. Furthermore, the voltage drop across the superconducting film is calculated from the difference between the surface-averaged scalar potential at the contacts, as described in [49]

$$V(t) = \langle\Phi\rangle_{\text{source}} - \langle\Phi\rangle_{\text{drain}}, \tag{3}$$

where $\langle\Phi\rangle_S = |S|^{-1}\int_S \Phi\, dS$ (with S, the surface of the sample). The **TDGL** equations are expressed in dimensionless units, with lengths scaled by the coherence length ξ, time by the Ginzburg–Landau characteristic time $t_{GL} = \pi\hbar/8k_BT_c$, magnetic fields by the upper critical field H_{c2} (field to which the superconductor transitions to a normal state), and the order parameter by its equilibrium value $\psi_\infty = \sqrt{-\alpha/\beta}$ [41, 43,46,50–52]. At the sample boundaries, we impose the generalized Neumann-de Gennes boundary condition $\hat{\mathbf{n}}\cdot(-i\nabla - \mathbf{A})\psi = -i\psi/b$, where $\hat{\mathbf{n}}$ is the outward normal vector and b is the extrapolation length [15,53, 54]. For insulating boundaries, we set $b \to \infty$ to ensure that the normal current is zero. These coupled equations are solved self-consistently using a finite-difference scheme on a two-dimensional mesh representing the superconducting film geometry, with convergence value $\epsilon = 10^{-8}$, for each numerical step, and we have used $\Delta x = 0.1$ for the space step. At the current-injection boundaries, $\hat{n}\cdot\nabla\mu = \pm\mathbf{J}_a$, where $\mathbf{J}_a$ is the applied current, while $\hat{n}\cdot\nabla\Phi = 0$ elsewhere [55–64]. Given the above, we proceed to present the numerical results.

3. Results

3.1. Cooper pair density

Initially, we present the Cooper-pair density for our proposed superconducting diode at different values of the applied external magnetic

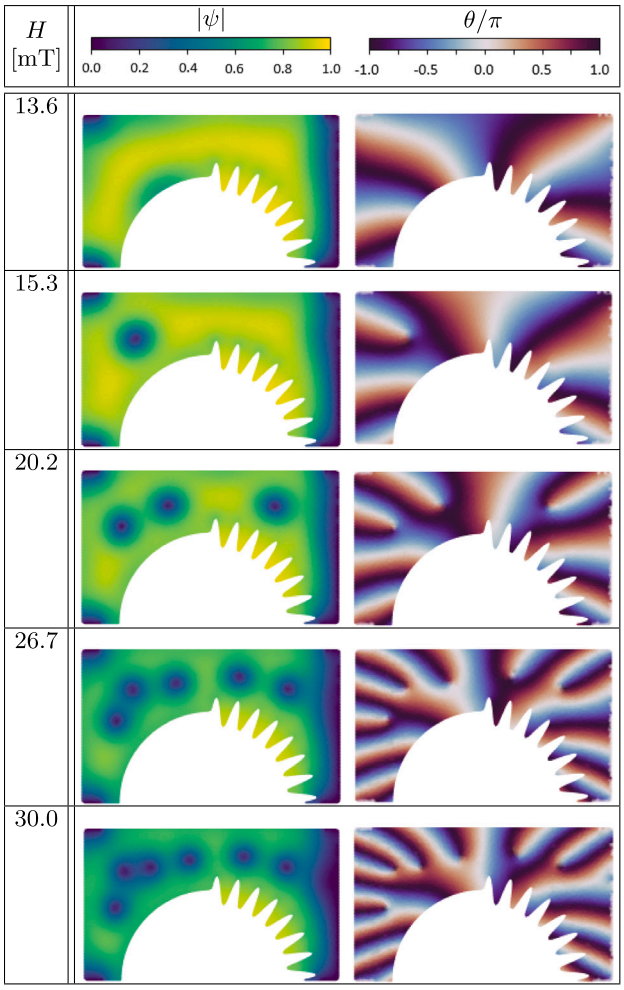


Fig. 2. Cooper pair density ($|\psi|^2$) and phase difference on the superconducting device with $\mathbf{J} = 0\,\mu\text{A}$ and $d = 0.4\,\xi$, as a function of the external applied magnetic field H.

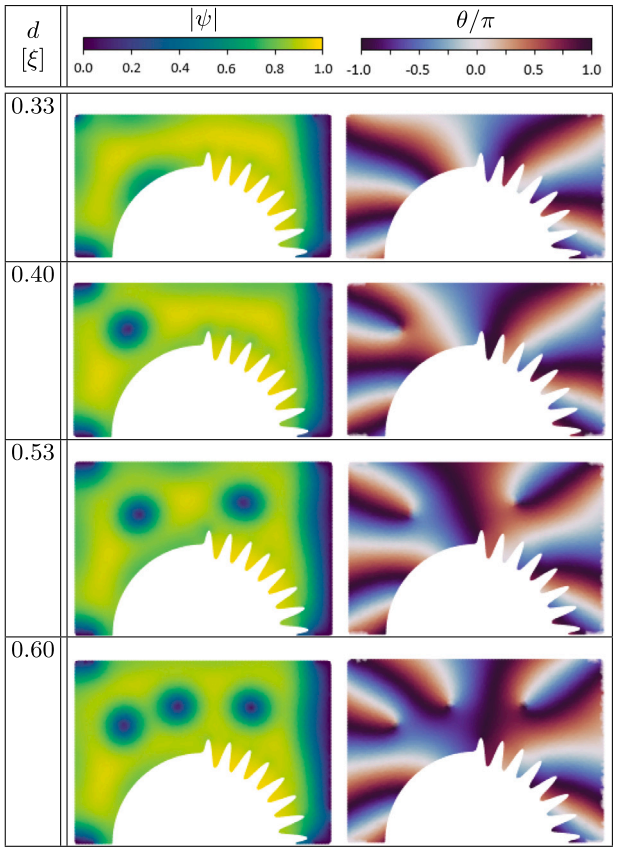


Fig. 3. Cooper pair density ($|\psi|^2$) and phase difference on the superconducting device under an applied magnetic field $H = 15.0$ mT and applied current $\mathbf{J} = 0$ μA, upon varying the bridge width.

field (H), in the presence of a constant applied current, with a constant value of the variable d (the bridge width). We use, the magnetic field H ranged in the interval from 13.6 mT to 30.0 mT. We present the results of this procedure in Fig. 2, since we are working with a Type II superconductor, here it is possible to observe within the first two values of H the transition between Meissner and mixed states, characterized by the entry of vortices in the film [65]; in particular, in the second value on the left, there is a suppression in $|\psi|^2$, of particular importance is the observation that the vortices enter through the section with greater symmetry (left), because the energy barrier on the non-symmetric side (right) has oscillations, which, when performing a non-linear superposition, tend to prevent the vortices from entering, along with the smaller amount of superconducting material in this same section [66,67]. In addition, as the external magnetic field increases, a greater number of vortices is observed in the sample. An asymmetry in the number of vortices is observed due to their monotonic repulsion, in conjunction with their interaction with the energy barrier at the boundary. Finally, in this same figure, we present the phase difference ($\psi = |\psi|e^{i\phi}$), where the color repetition indicates a change of 2π; this clearly indicates the presence of a vortex in the superconducting sample, furthermore, it is evident that there is an increase in phase changes, and the differences between the phases in the superconductor sections are apparent.

With this, in Fig. 3 we present the second situation, where the bridge width d takes values between $0.33\,\xi$ and $0.6\,\xi$, with a constant current density $\mathbf{J} = 0\,\mu\text{A}$ and a constant magnetic field of $H = 15\,\text{mT}$. Taking into account that the radius of the defect R is held constant, it is worth noting that the increment of the bridge width in these graphs can also be seen as the increment of the vertical side of the film. From these Cooper densities, a transition between the Meissner and mixed states can be inferred as in the previous case, demonstrating that a geometrical parameter such as this also affects how vortices interact with the film. However, the transition that occurs between $d = 0.33\,\xi$ and $d = 0.4\,\xi$. This is because the bridge's size induces oscillations in the energy barrier, favoring the entry of these vortices for larger d, as the magnetic pressure decreases with d.

To conclude this analysis of Cooper densities, we present this density precisely for both polarities of the applied external current, as well as in the absence of current, using the same value of the bridge width variable d. In Fig. 4, its spatial distribution is shown for a magnetic field of $H = 13.0\,\text{mT}$ and a bridge width of $d = 0.4\xi$. The current density $\mathbf{J}$ changes within the symmetric interval $[-0.02, 0.02]$ in units of μA. Setting the current to zero as a reference, we observe the formation of well-known phase slips. In the case of positive current, phase slips predominantly form in the circular section (left), where rapid kinematic vortex movement can occur without large spatial variations. In contrast, the right section contains defects, and their energy barrier hinders this rapid movement. For negative current, phase slips are again observed in the most symmetrical section at low current values. However, at very high values of the applied external current, they occur only in the circular section. The difference in Cooper-pair density is now evident for the same current but in different directions (first and last panels). This result stems from breaking spatial symmetry in the sample and provides evidence that the vortex distribution in the superconducting sample is responsible for the superconducting

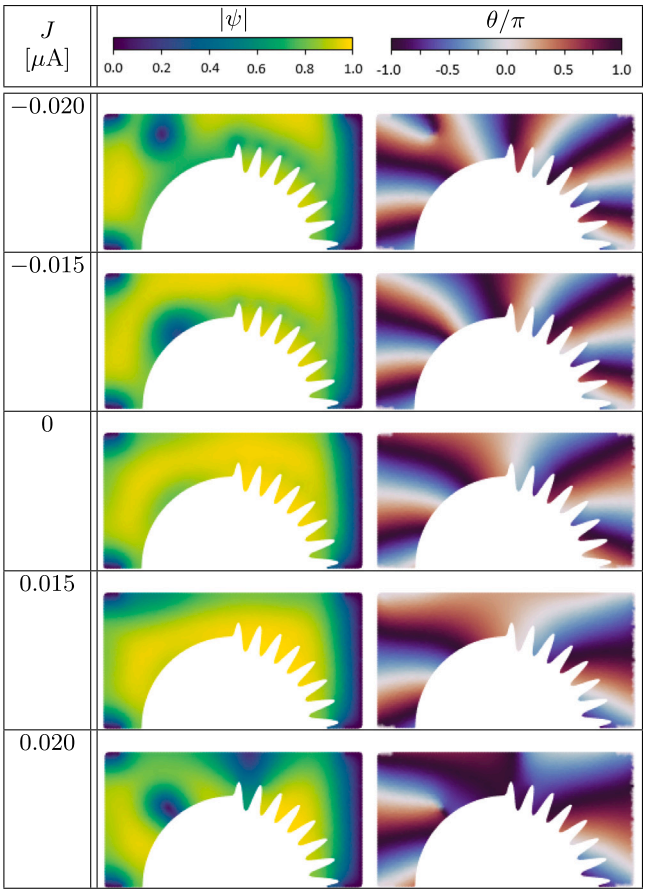


Fig. 4. Cooper pair density ($|\psi|^2$) and phase difference on the superconducting device in an applied magnetic field $H = 13.0$ mT, varying the applied current **J** and keeping a value $d = 0.4\,\xi$.

diode effect (**SDE**). This evidence is reinforced by the phase difference between the same panels, revealing differences in both the number and position of vortices in the sample.

This concludes the study of the Cooper pair density for the three main cases. Therefore, we will study the electronic variables, specifically the efficiency parameter, of the superconducting diode model we propose.

3.2. V-I curves and SDE

In this section, we present the scalar potential curves for fixed values of the external magnetic field H. We show both polarities of the applied external current **J**, where the potential in the sample is calculated using Eq. (3). We use a constant value for the bridge thickness $d = 0.27\xi(0)$, as studied in the exterior section. Initially, in Fig. 5, we observe zero crossings in these scalar potential curves, followed by jumps (Shapiro jumps). These jumps describe the entry of one of two types of vortices: kinematic or Abrikosov. Kinematic vortices originate from oscillations in the phase of the superconducting condensate caused by the application of external currents. Abrikosov vortices, on the other hand, arise due to an increase in the external magnetic field, which allows regions of the normal state to coexist with the superconducting state. In Fig. 5, we present the behavior of the scalar potential for different magnetic field values. As expected, the Shapiro jump occurs at lower values of the external current as the magnetic field increases. This results from the suppression of the interaction between the applied current and the super-current, arising from the coordinated motion of the Cooper-pair density. An important

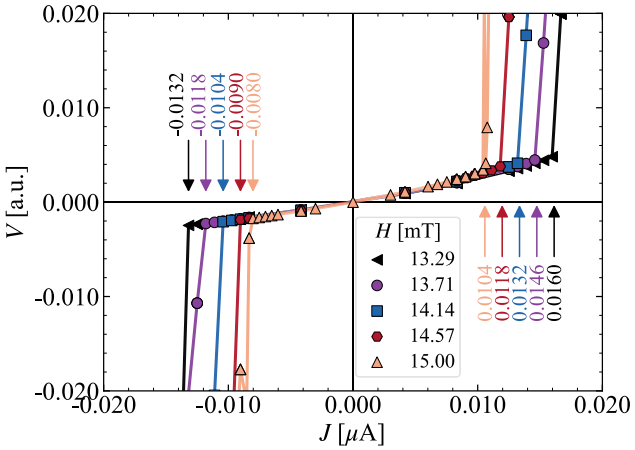


Fig. 5. Scalar potential (V) obtained in the sample from applied currents **J** for different values of the external magnetic field (H). The value of the bridge width corresponds to $d = 0.27\,\xi(0)$. The vertical dashed lines represent the locations of the first critical currents (First Shapiro step). The exact values at which the jumps occur are shown in the figure for both polarities.

observation is the lack of symmetry between the curves for both current polarities, indicating asymmetry in this electronic variable. A method used in recent years to describe the diode's efficiency that involves determining the critical (first) current densities in both directions. In this context, these will be denoted as J_c^+ (left to right) and J_c^- (right to left), and then calculating an efficiency parameter (or diode efficiency) defined as [68–70]:

$$\gamma(H) = \left(\frac{|J_c^+(H) - |J_c^-(H)||}{J_c^+(H) + |J_c^-(H)|} \right) \times 100 \tag{4}$$

The critical currents, and thus the diode efficiency, depend on key parameters. In this study, we focus on two variables: the applied magnetic field H and the bridge width d, which were varied in prior simulations. Since **SDE** requires time-inversion symmetry breaking [71–91], enabled by the external magnetic field, a Lorentz force arises when current is applied. This, in turn, drives vortex motion in the sample, as shown in Figs. 2–4, where a line of reduced Cooper pair density appears. In Fig. 6(a), we present the magnitude of the first critical currents (first Shapiro jump) as a function of the applied magnetic field. The range examined is from 12.0 to 15.0 mT. These current values coincide only at 12.0 and 12.6 mT. For other field values, the critical currents differ in magnitude. This difference indicates a change in symmetry, as evidenced by the superconducting system we are studying. For higher values of the external magnetic field, the currents equalize. Although there is a break in symmetry, the system is then forced to transition to a normal state, reducing the critical currents to zero. Special emphasis is placed on graphing specific indicators with red dots to highlight differences in the y-axis variable.

Now, having presented the magnitudes of the first critical currents, in Fig. 6(b) we present the efficiency of the proposed superconducting diode, this value $\gamma(H)$, presents different values, ranging from a zero efficiency at 12.0 mT, followed by a non-monotonic but ascending behavior, presenting a maximum efficiency of 13.2% after which descends rapidly and returns again to a null value, for higher values of the external field. Thus, the superconductor system exhibits diode-type efficiency for fixed values of the external magnetic field, allowing the determination of the efficiency and making the hand sign of this system particularly efficient. We now present the variation in the bridge width for a constant magnetic field. Thus, in Fig. 7 there are four $V - I$ curves for different bridge widths d, taking values from $0.23\,\xi(0)$ to $0.33\,\xi(0)$, at a constant applied magnetic field of 14 mT, which we took, because in the previous study we noted that it had a high efficiency value and

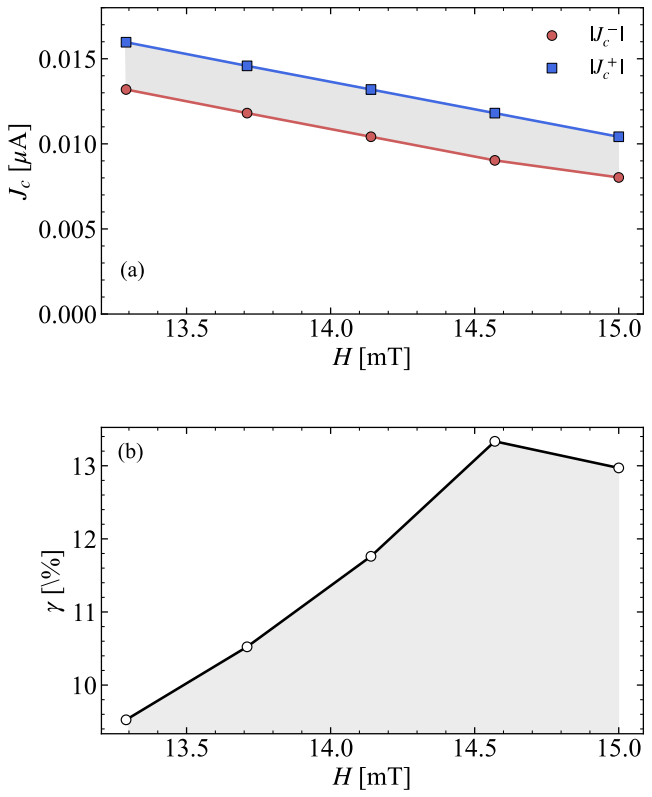


Fig. 6. (a) Magnitude of the first critical (First Shapiro step) currents with opposite polarization as a function of the applied magnetic field. (b) Efficiency factor $\gamma(H)$ as a function of the applied magnetic field H, for a fixed value of $d = 0.27\,\xi(0)$.

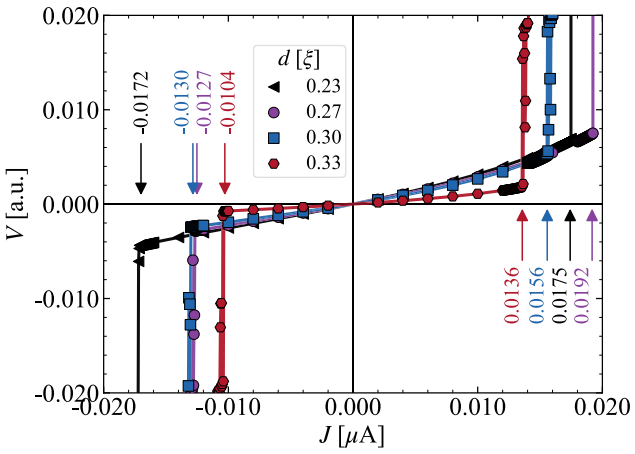


Fig. 7. Scalar potential (V) obtained in the sample from applied currents **J** for different bridge-width values d, while maintaining an external magnetic field $H = 13$ mT. The vertical dashed lines represent the locations of the critical currents. The exact values at which the jumps occur are shown in the figure for both polarities.

tended to increase, without reaching the maximum, we have made a graph for the two different polarities of the external current, we observe the quasi-zero behavior, for low values of the applied external current, which is indicative of the resistance to the entry of the magnetic field (Meissner state), after which, the Shapiro jumps are quickly observed, and it is evident that for higher values of the parameter d, the currents are lower, because having a greater amount of material, the energy barrier is lower and the entry of kinematic and Abrikosov type vortices is facilitated. Therefore, as the size decreases, the competition between the currents (superconducting and external), together with the Lorentz force, tends to generate a non-linear superposition, making it more difficult to overcome this energy barrier.

The magnitude of the critical current densities as a function of $d \in [0.2\,\xi, 0.37\,\xi]$ for both polarities was also obtained from the $V - I$ curves, where to determine $J_c^{\pm}$ with better precision, more points were calculated around these critical values, this can be seen in Fig. 7 noting the increase of the density points near vertical lines. The results are plotted in Fig. 8(a). An analysis of $|J_c^+|$ and $|J_c^-|$ with this graph validates the affirmations made before; neither the positive nor the negative polarity exhibits a linear behavior, and over the range studied here, they are non-monotonic. Additionally, comparing these two curves, it is clear that the critical currents change in different ways without a pattern; both values can increase and decrease over some intervals, but they can also change in opposite directions at other times. This result, besides demonstrating the presence of **SDE** in the film, also confirms that this geometric parameter has a strong influence on the asymmetry of the critical currents and, consequently, on the **SDE** itself.

The **SDE** efficiency as a function of the bridge width ($\gamma(d)$) is presented in Fig. 6(b) in the same domain as Fig. 8. As it was expected from the form of $|J_c^+|$ and $|J_c^-|$, $\gamma(d)$ does not follow a simple explicit behavior and it rather validates the affirmation that this sample is highly sensitive to variations of d, indicated by the abrupt changes of the efficiency for relatively small variations of the bridge width. In particular, using the simulated data points, the most extreme scenario occurs between $d = 0.23\,\xi$ and $d = 0.27\,\xi(0)$, where the efficiency changes from a value of approximately 1.2% to a 21%, the minimum and maximum obtained in this range, respectively. Moreover, this second value shows that with the right choice of d, the sample can achieve high efficiency, underscoring the importance of analyzing this parameter when designing the device to obtain an appreciable **SDE**. This great and accurate change in the bridge size, due to the competition between the currents at the points of greater symmetry in the superconducting sample, is observed. The competing currents are the one due to Cooper pairs, the external current, and the one that creates the Lorentz force. Given this, at a specific size, the greatest shielding is achieved, thereby reducing the local energy barrier. As a final remark of this section, we can highlight the fact that these results suggest that an asymmetric response from a bi-dimensional sample can be obtained purely by modifying its boundaries, without the necessity of Josephson junctions or spin–orbit coupling. Breaking spatial inversion symmetry by this method and time-reversal symmetry with an external magnetic field offers an interesting way to obtain a wide range of SDE efficiencies in these mesoscopic films.

This concludes the study of our proposal for a superconducting diode. Notably, we observe that greater efficiency can be achieved by varying the bridge width, exceeding 20%. If this designer is complemented, higher values of this efficiency are expected at low applied magnetic field values. Now, the advantages of this design are clearly its manufacturing, which does not imply carrying out multi-band or multi-condensate extensions, which increase manufacturing costs, and of course, in the theoretical study, involves multi-condensate systems that increase the number of computational processes, but only with a break in symmetry allows its implementation and design. In addition, the study has been carried out so that the values of the present work can be implemented in the laboratory, and finally, it is important to highlight that the study has been carried out in the fine limit, without making use of 3-dimensional extensions that complicate the theoretical analysis and manufacturing much more.

4. Conclusions

In this study, we simulated and analyzed the behavior of a mesoscopic film. Its shape breaks spatial inversion symmetry due to a defect

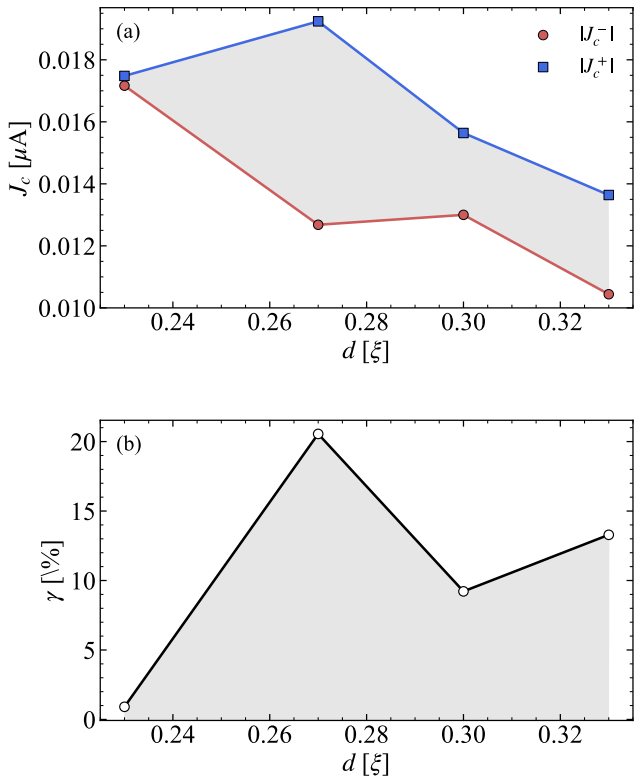


Fig. 8. (a) Magnitude of the first critical currents (first Shapiro step) with opposite polarization as a function of the bridge width, for a fixed external magnetic field as a function of the external current. (b) Efficiency factor $\gamma(d)$ as a function of the bridge width d, for a fixed value of $H = 14\,\mathrm{mT}$ and external applied current **J**.

on one side of the slab. We numerically solved the time-dependent Ginzburg–Landau equation to obtain the order parameter $\psi(\mathbf{r}, t)$ and the Cooper-pair density $|\psi(\mathbf{r}, t)|^2$. The study demonstrates an unconventional configuration of vortices arising from spatial variations in the energy barrier, thereby creating asymmetric sample boundaries. Because the vortices have different configurations, they affect the efficiency of the proposed sample. We calculate the average of the scalar potential (voltage (V)) between two points as we vary the applied magnetic field (H), the bias current density (**J**), and a geometrical parameter. As the magnetic field increases while other parameters remain constant, the values of the Shapiro jumps decrease, indicating that vortex entry into the sample becomes easier and reduces control over critical current densities. This indicates a decline in device efficiency, directly related to vortex-symmetry breaking. Notably, these critical currents are not symmetrical with respect to the polarity of the applied current. From the measurements, we determined critical current densities for opposite polarities and the characteristic superconducting diode efficiency $\gamma(H)$. We observe a maximum value for a specific parameter combination (13.4%), after which it decreases. This result clearly indicates that a privileged configuration exists for this variation, emphasizing the importance of optimizing geometry and field conditions to maximize diode efficiency and enabling controlled control of vortex states.

Finally, $V-I$ curve measurements, together with the critical current values for both polarities, which allow calculating the efficiency factor of the superconducting diode effect efficiency $\gamma(d)$, again present a configuration in which there is a higher value of this parameter. With this, the superconducting diode uses optimal data from both variations, thereby increasing its overall efficiency. An efficiency of 20% was achieved — a high value for this parameter — solely by varying the geometry of the sample. Calculations show that the superconducting diode effect can be obtained purely from spatial asymmetry, without the need for Josephson junctions or modifications to the Ginzburg–Landau equation. Therefore, this work provides useful evidence that boundary geometry is relevant to designing highly efficient, low-cost superconducting diodes, as it avoids the use of complex, expensive multi-condensing systems.

CRediT authorship contribution statement

C.A. Aguirre: Methodology, Investigation, Formal analysis, Data curation, Conceptualization. **Julián Faúndez:** Methodology, Data curation, Conceptualization. **S.A. Acosta-Díaz:** Methodology, Formal analysis, Data curation, Conceptualization. **C.E. Martínez-Torres:** Methodology, Investigation, Formal analysis, Data curation, Conceptualization. **J. Barba-Ortega:** Methodology, Investigation, Funding acquisition, Formal analysis, Data curation, Conceptualization.

Declaration of competing interest

The authors declare that they have no known competing financial interests or personal relationships that could have appeared to influence the work reported in this paper.

Acknowledgments

C. Aguirre thanks S. Aguirre and M. Aguirre for useful discussions. C. Aguirre thanks the CNPq grant number process: 174045/2023-9 for financial support. J. Fáundez acknowledges the support from ANID Fondecyt grant number 3240320. Powered@NLHPC: This research was partially supported by the NLHPC super-computing infrastructure (CCSS210001). J.Barba-Ortega thaks Alejandro and Marcos by useful discussions.

Data availability

Data will be made available on request.

References

[1] C. Ye, J. Che, T. Han, H. Huang, Multi-band analysis on physical properties of the quasi-two-dimensional superconductor $NbSe_2$, Coatings 13 (3) (2023) 548.
[2] P. Holmvall, A.M. Black-Schaffer, Coreless vortices as direct signature of chiral d-wave superconductivity, Phys. Rev. B 108 (2023) L100506.
[3] K. Jiang, T. Wu, J.X. Yin, Z. Wang, M.Z. Hasan, S.D. Wilson, X. Chen, J. Hu, Kagome superconductors AV_3Sb_5 (A=K, Rb, Cs), Nat. Sci. Rev. 10 (2) (2023).
[4] J. Bekaert, A. Aperis, B. Partoens, P.M. Oppeneer, M.V. Milošević, Advanced first-principles theory of superconductivity including both lattice vibrations and spin fluctuations: The case of FeB_4, Phys. Rev. B 97 (2018) 014503.
[5] C.A. Aguirre, J. Barba-Ortega, A.S. de Arruda, J. Faundez, Superconducting diode effect in a meso-wedge geometry with Abrikosov vortices, SciPost Phys. Core 9 (2026) 006.
[6] A. Kapustin, L. Mrini, Universal time-dependent Ginzburg-Landau theory, Phys. Rev. B 107 (2023) 144514.
[7] W.D. Gropp, H.G. Kaper, G.K. Leaf, D.M. Levine, M. Palumbo, V.M. Vinokur, Numerical simulation of vortex dynamics in type-II superconductors, J. Comput. Phys. 123 (1996) 254–266.
[8] H.J. Fink, A.G. Presson, Magnetic irreversible solution of the Ginzburg-Landau equations, Phys. Rev. 151 (1967) 219–227.
[9] J.J. Palacios, Vortex matter in superconducting mesoscopic disks: Structure, magnetization, and phase transitions, Phys. Rev. B 58 (1998) R5948–R5951.
[10] I. Timoshuk, E. Babaev, Microscopic solutions for vortex clustering in two-band type-1.5 superconductors, Phys. Rev. B 110 (2024) 064509.
[11] A. Talkachov, S. Kaushik, E. Babaev, Microscopic approach to the problem of enhancement and suppression of superconductivity on twinning planes, Phys. Rev. B 111 (2025) 054513.
[12] E.A. Teplyakov, V.G. Yarzhemsky, Space-group approach to the Ginzburg–Landau phase winding in topological superconductors: Application to Sr_2RuO_4, J. Phys.: Condens. Matter. 37 (2025) 185705.

[13] M. Mootz, L. Luo, C. Huang, J. Wang, L.E. Perakis, Multidimensional coherent spectroscopy of light-driven states and their collective modes in multiband superconductors, Phys. Rev. B 109 (2024) 014515.

[14] K. Hauser, A. Villegas, Theory of pseudospin resonance for multiband superconductors, Phys. Rev. B 108 (2023) 174504.

[15] C. Aguirre, J. Barba-Ortega, A. de Arruda, P. Díaz, C. Cortés, D. Laroze, Study of a possible superconducting 3D diode via reflection symmetry breaking, Phys. B 720 (2026) 417960.

[16] N.H. Aase, K. Mæland, A. Sudbø, Multiband strong-coupling superconductors with spontaneously broken time-reversal symmetry, Phys. Rev. B 108 (2023) 214508.

[17] H. Xu, C.-M. Chung, M. Qin, U. Schollwöck, S.R. White, S. Zhang, Coexistence of superconductivity with partially filled stripes in the hubbard model, Science 384 (2024) eadh7691.

[18] E.V. Ramirez, L. Becerra-Londono, M.R. Joya, J. Barba-Ortega, C.A. Aguirre, Vortex matter in superconducting films with different nanopatterns, Int. J. Mod. Phys. B 40 (2026) 2650028.

[19] J.E. González, O.A. González-Estrada, J. Barba-Ortega, Vortex and anti-vortex states in superconducting membrane with structural anomalies, Appl. Phys. A 132 (2025) 79.

[20] A. Chaves, F.M. Peeters, G.A. Farias, M.V. Milošević, Vortex-vortex interaction in bulk superconductors: Ginzburg-Landau theory, Phys. Rev. B 83 (2011) 054516.

[21] Y. Wang, M. Li, C. Pei, L. Gao, K. Bu, D. Wang, X. Liu, L. Yan, J. Qu, Critical current density and vortex phase diagram in the superconductor, Phys. Rev. B 106 (2022) 054506.

[22] S. Kozlov, J. Lesueur, D.R. et al., Dynamic metastable vortex states in interacting vortex lines, Commun. Phys. 7 (2024) 183.

[23] R. Wördenweber, P. Dymashevski, V.R. Misko, Guided vortex motion in superconductors with asymmetric pinning landscapes, Phys. Rev. B 69 (2004) 184504.

[24] T. Golod, A. Pagliero, V.M. Krasnov, Two mechanisms of Josephson phase shift generation by an Abrikosov vortex, Phys. Rev. B 100 (2019) 174511.

[25] B. Pal, P. Chakraborty, A. Sivakumar, P. K., et al., Josephson diode effect from cooper pair momentum in a topological semimetal, Nat. Phys. 18 (2022) 1228–1233.

[26] M. Davydova, S. Prembabu, L. Fu, Universal Josephson diode effect, Sci. Adv. 8 (2022) eabo0309.

[27] J. Ma, R. Zhan, X. Lin, Superconducting diode effects: Mechanisms, materials and applications, Adv. Phys. Res. 4 (6) (2025).

[28] M. Castellani, O. Medeiros, A. Buzzi, et al., A superconducting full-wave bridge rectifier, Nat. Electron. 8 (2025) 417–425.

[29] J. Ingla-Aynés, Y. Hou, S. Wang, et al., Efficient superconducting diodes and rectifiers for quantum circuitry, Nat. Electron. 8 (2025) 411–416.

[30] T. Golod, V. Krasnov, Demonstration of a superconducting diode-with-memory, operational at zero magnetic field with switchable nonreciprocity, Nat. Commun. 13 (2022) 3658.

[31] I.I. Soloviev, N.V. Klenov, S.V. Bakurskiy, M.Y. Kupriyanov, A.L. Gudkov, A.S. Sidorenko, Beyond Moore's technologies: Operation principles of a superconductor alternative, Beilstein J. Nanotechnol. 8 (2017) 2689–2710.

[32] Y. Cheng, Q. Shu, H. He, B. Dai, K.L. Wang, Current-driven magnetization switching for superconducting diode memory, Adv. Mater. 37 (11) (2025) 2415480.

[33] Supercurrent rectification and magnetochiral effects in symmetric Josephson junctions, SNature Nanotechnol. 17 (14) (2022) 39.

[34] Y. Miyasaka, R. Kawarazaki, H. Narita, F. Ando, Y. Ikeda, R. Hisatomi, A. Daido, Y. Shiota, T. Moriyama, Y. Yanase, T. Ono, Observation of nonreciprocal superconducting critical field, Appl. Phys. Express 14 (1) (2021) 073003.

[35] H. Narita, J. Ishizuka, R. Kawarazaki, D. Kan, Y. Shiota, T. Moriyama, Y. Shimakawa, A. Ognev, A. Samardak, Y. Yanase, T. Ono, Field-free superconducting diode effect in noncentrosymmetric superconductor/ferromagnet multilayers, Appl. Phys. Express 17 (1) (2022) 823–828.

[36] K. Yasuda, H. Yasuda, T. Liang, R. Yoshimi, A. Tsukazaki, K. Takahashi, N. Nagaosa, M. Kawasaki, Y. Tokura, Nonreciprocal charge transport at topological insulator/superconductor interface, Nature Commun. 10 (1) (2019) 2734.

[37] D. Cerbu, V.N. Gladilin, J. Cuppens, J. Fritzsche, J. Tempere, J.T. Devreese, V.V. Moshchalkov, A.V. Silhanek, J. Van De Vondel, Vortex ratchet induced by controlled edge roughness, New J. Phys. 15 (6) (2013) 063022.

[38] F. Porrati, A.O. Pokusinskyi, S. Barth, M. Huth, O.V. Dobrovolskiy, Vortex ratchet effect in a NBC strip with a periodic edge indentation, Small Methods 9 (12) (2025) e01430.

[39] C. Reichhardt, C.J.O. Reichhardt, Moving vortex phases, dynamical symmetry breaking, and jamming for vortices in honeycomb pinning arrays, Phys. Rev. B 78 (2008) 224511.

[40] W. Gillijns, A.V. Silhanek, V.V. Moshchalkov, Origin of reversed vortex ratchet motion, Phys. Rev. Lett. 99 (2007) 247002.

[41] Y. Zhang, Y. Gu, P. Li, J. Hu, K. Jiang, General theory of Josephson diodes, Phys. Rev. X 12 (2022) 041013.

[42] J. Hasan, D. Shaffer, M. Khodas, A. Levchenko, Superconducting diode efficiency from singlet-triplet mixing in disordered systems, Phys. Rev. B 111 (2025) 174514.

[43] S. Qi, J. Ge, C. Ji, Y. Ai, G. Ma, Z. Wang, Z. Cui, Y. Liu, Z. Wang, J. Wang, High-temperature field-free superconducting diode effect in high-T_c cuprates, Nat. Commun. 16 (2025) 531.

[44] I. de M. Froldi, H. Freire, Efficiency of the superconducting diode effect of pair-density-wave states in two-dimensional d-wave altermagnets, Ann. Phys. 483 (2025) 170273.

[45] X. Zeng, R. Zhang, G. Guo, Z. Gao, Q. Hu, H. Ji, F. Yang, X. Wang, B. Gao, N.F.Q. Yuan, B. Lv, X. Liu, H. Ding, Large superconducting diode effect driven by edge states in twisted iron-chalcogenide josephson junctions, 2025, arXiv arXiv:2510.00595.

[46] D. Chakraborty, A.M. Black-Schaffer, Perfect superconducting diode effect in altermagnets, Phys. Rev. Lett. 135 (2025) 026001.

[47] J.J. He, Y. Tanaka, N. Nagaosa, A phenomenological theory of superconductor diodes, New J. Phys. 24 (2022) 053014.

[48] L.D. Anh, K. Ishihara, T. Hotta, K. Inagaki, H. Maki, T. Saeki, M. Kobayashi, M. Tanaka, Large superconducting diode effect in Sn-based nanowire/topological Dirac semimetal heterostructures, Nat. Commun. 15 (2024) 8014.

[49] H. Huang, T. de Picoli, J.I. Väyrynen, Superconducting diode effect in two-dimensional topological insulator edges and Josephson junctions, Appl. Phys. Lett. 125 (2024) 032602.

[50] F. Liu, Y.M. Itahashi, S. Aoki, Z. D., N. Ogawa, T. Ideue, Y. Iwasa, Superconducting diode effect under time-reversal symmetry, Sci. Adv. 10 (2024) eado1502.

[51] S. Banerjee, M.S. Scheurer, Altermagnetic superconducting diode effect, Phys. Rev. B 110 (2024) 024503.

[52] R. Sharma, H.K. Meena, Emerging trends in EEG signal processing: A systematic review, SN Comput. Sci. 5 (2024) 415.

[53] Q. Du, M. Gunzburger, A model for superconducting thin films having variable thickness, Phys. D 69 (1993) 215–231.

[54] K. Jiang, J. Hu, Superconducting diode effects, Nat. Phys. 18 (2022) 1145.

[55] P.J.W. Moll, Geometrical design of 3D superconducting diodes, Commun. Mater. 6 (2025) 73.

[56] L.Z. Deng, Z. Wu, T. Bontke, T. Habamahoro, D. Schulze, M. Gooch, T.W. Kuo, R. Fujikawa, C.W. Chu, From high-temperature superconductivity to room-temperature superconductivity, IOP Conf. Ser.: Mater. Sci. Eng. 1302 (2023) 012010.

[57] V.V. Moshchalkov, M. Menghini, T. Nishio, Q.H. Chen, A.V. Silhanek, V.H. Dao, L.F. Chibotaru, N.D. Zhigadlo, J. Karpinski, Type-1.5 Superconductivity, Phys. Rev. Lett. 102 (2009) 117001.

[58] L.R. Cadorim, A.R. de C. Romaguera, I.G. de Oliveira, R.R. Gomes, M.M. Doria, E. Sardella, Intermediate type-I superconductors in the mesoscopic scale, Phys. Rev. B 103 (2021) 014504.

[59] M. Nadeem, M.S. Fuhrer, X. Wang, The superconducting diode effect, Nat. Rev. Phys. 5 (2023) 558–577.

[60] C.A. Aguirre, P. Díaz, D. Laroze, A.S.M. Polo, J. Barba-Ortega, Vortex state in a 3D superconducting mesoscopic wedge, Physica C 618 (2024) 1354450.

[61] Ž.L. Jelić, M.V. Milošević, A.V. Silhanek, Velocimetry of superconducting vortices based on stroboscopic resonances, Sci. Rep. 6 (2016) 35687.

[62] A. Gutfreund, H. Matsuki, V. Plastovets, A. Noah, L. Gorzawski, N. Fridman, G. Yang, A. Buzdin, O. Millo, J.W.A. Robinson, Y. Anahory, Direct observation of a superconducting vortex diode, Nat. Commun. 14 (2023) 1630.

[63] M. Castellani, O. Medeiros, A. Buzzi, A. Foster, M. Colangelo, K.K. Berggren, A superconducting full-wave bridge rectifier, Nat. Electron. 8 (2025) 417–425.

[64] T. Golod, V.M. Krasnov, Demonstration of a superconducting diode-with-memory, Nat. Commun. 13 (2022) 3658.

[65] E. Thoeng, M. Asaduzzaman, P. Kolb, R.M.L. McFadden, G.D. Morris, J.O. Ticknor, S.R. Dunsiger, V.L. Karner, D. Fujimoto, T. Junginger, R.F. Kiefl, W.A. MacFarlane, R. Li, S. Saminathan, R.E. Laxdal, Depth-resolved characterization of meissner screening breakdown in surface treated niobium, Scientific Rep. 14 (1) (2024) 21487.

[66] T. Ueda, Y. Sera, H. Adachi, M. Ichioka, Nonmagnetic impurity effect in vortex states of chiral superconductors, Phys. Rev. B 103 (1) (2021) 014506.

[67] A.J. Beekman, J. Zaanen, Electrodynamics of Abrikosov vortices: The field theoretical formulation, Front. Phys. 6 (4) (2011) 357–369.

[68] S. Banerjee, M.S. Scheurer, Altermagnetic superconducting diode effect, Phys. Rev. B 110 (2024) 024503.

[69] N.F.Q. Yuan, L. Fu, Supercurrent diode effect and finite-momentum superconductors, Proc. Natl. Acad. Sci. 119 (15) (2022) e2119548119.

[70] S. Ilić, F.S. Bergeret, Theory of the supercurrent diode effect in Rashba superconductors with arbitrary disorder, Phys. Rev. Lett. 128 (2022) 177001.

[71] J.J. He, Y. Tanaka, N. Nagaosa, A phenomenological theory of superconductor diodes, New J. Phys. 24 (5) (2022) 053014.

[72] M. Nadeem, M.S. Fuhrer, X. Wang, The superconducting diode effect, Nat. Rev. Phys. 5 (10) (2023) 558–577.

[73] T. Karabassov, I.V. Bobkova, V.M. Silkin, B.G. Lvov, A.A. Golubov, A.S. Vasenko, Phase diagrams of the diode effect in superconducting heterostructures, Phys. Scr. 99 (1) (2023) 015010.

[74] S. Ilić, P. Virtanen, D. Crawford, T.T. Heikkilä, F.S. Bergeret, Superconducting diode effect in diffusive superconductors and Josephson junctions with Rashba spin-orbit coupling, Phys. Rev. B 110 (2024) L140501.

[75] Y. Mao, Q. Yan, Y.-C. Zhuang, Q.-F. Sun, Universal spin superconducting diode effect from spin-orbit coupling, Phys. Rev. Lett. 132 (2024) 216001.
[76] H. Narita, J. Ishizuka, R. Kawarazaki, D. Kan, Y. Shiota, T. Moriyama, Y. Shimakawa, A.V. Ognev, A.S. Samardak, Y. Yanase, T. Ono, Field-free superconducting diode effect in noncentrosymmetric superconductor/ferromagnet multilayers, Nature Nanotechnology 17 (8) (2022) 823–828.
[77] H. Huang, T. de Picoli, J. Väyrynen, Superconducting diode effect in two-dimensional topological insulator edges and Josephson junctions, Appl. Phys. Lett. 125 (3) (2024).
[78] L. Bishop-Van Horn, pyTDGL: Time-dependent Ginzburg–Landau in Python, Comput. Phys. Communications 291 (2023) 108799.
[79] D. Stosic, High-Performance Ginzburg-Landau Simulations of Superconductivity (Ph.D. thesis), Universidade Federal de Pernambuco and University of Antwerp, Recife, Brazil, 2018.
[80] J.E. Gonzalez-Balaguera, C.A. Aguirre, J. Barba-Ortega, Roundabout-like defect as a guide of phase-slip lines in a superconducting thin film at low temperature, Emergent Materials 7 (2024) 1975–1982.
[81] A. He, C. Xue, H. Yong, Y. Zhou, The guidance of kinematic vortices in a mesoscopic superconducting strip with artificial defects, Supercond. Sci. Technol. 29 (6) (2016) 065014.
[82] A. He, C. Xue, H. Zhang, Q. Deng, Y.H. Zhou, The position-dependent vortex dynamics in the asymmetric superconducting ring, AIP Adv. 7 (4) (2017) 045304.
[83] G. Carapella, V. Granata, F. Russo, G. Costabile, Bistable Abrikosov vortex diode made of a Py–Nb ferromagnet-superconductor bilayer structure, Appl. Phys. Lett. 94 (2009) 242504.
[84] B. Chesca, D. John, R. Pollett, M. Gaifullin, J. Cox, C.J. Mellor, S. Savelev, Magnetic field tunable vortex diode made of $YBa_2Cu_3O_{7-\delta}$ Josephson junction asymmetrical arrays, Appl. Phys. Lett. 111 (2017) 062602.
[85] C. Wang, G. Hu, X. Ma, H. Tan, J. Wu, Y. Feng, S. Wang, R. Li, B. Zheng, J.J. He, B. Xiang, Superconducting-diode effect induced by inversion-symmetry breaking in a stepped $NbSe_2$ nanoflake, Phys. Rev. Appl. 22 (2024) 064017.
[86] J. Cayao, N. Nagaosa, Y. Tanaka, Enhancing the Josephson diode effect with Majorana bound states, Phys. Rev. B 109 (2024) L081405.
[87] R.S. Souto, M. Leijnse, C. Schrade, Josephson diode effect in supercurrent interferometers, Phys. Rev. Lett. 129 (2022) 267702.
[88] A. Costa, O. Kanehira, H. Matsueda, J. Fabian, Unconventional Josephson supercurrent diode effect induced by chiral spin-orbit coupling, Phys. Rev. B 111 (2025) L140506.
[89] F. Ando, Y. Miyasaka, T. Li, J. Ishizuka, T. Arakawa, Y. Shiota, T. Moriyama, Y. Yanase, T. Ono, Observation of superconducting diode effect, Nature 584 (2020) 373–376.
[90] M. Buchacek, Z.L. Xiao, S. Dutta, E.Y. Andrei, P. Raychaudhuri, V.B. Geshkenbein, G. Blatter, Experimental test of strong pinning and creep in current-voltage characteristics of type-II superconductors, Phys. Rev. B 100 (2019) 224502.
[91] L. Horng, R. Cao, T.C. Wu, S. Yang, S.H. Wang, J.C. Wu, T.J. Yang, Experimental and simulation study of pinning phenomena in superconductors with regular composite pinning arrays, J. Appl. Phys. 113 (2013) 17E118.